Implementation aspects of elastic FWI and its application to sparse OBN surveys

Cosmin Macesanu, Faqi Liu, Yi Huang, Hao Hu and Carlos Calderón, TGS*

Summary

Full waveform inversion employing finite differences (FD) modeling is a commonly-used tool for deriving high resolution velocity models. Sparse Ocean Bottom Node (OBN) acquisition leverages this method effectively, offering a cost-effective solution in areas of complex geology where long to super-long offsets and full azimuth sampling are needed for reducing the uncertainty of the derived model and image. Most applications of FWI with this type of data are in the acoustic limit, but accounting for the elasticity of the earth can result in a higher fidelity in simulating the real data and hence accelerate convergence. However, the FD method poses computational challenges in areas with strong inhomogeneity, where using the elastic approach is most beneficial. In this work we discuss some of the computational challenges for accurately modeling the elastic wavefield in presence of strong contrast media. We illustrate our findings with results from a super-long offset, sparse OBN survey from the Gulf of México, which highlight the benefits provided by using the full elastic equations versus the acoustic approximation.

Introduction

Acoustic Full Waveform Inversion (FWI) has been the preferred method for building accurate velocity models, especially for low-frequency and long offset acquisitions. FWI inverts for a velocity model which generates synthetic data that best matches the field data. The success of this method has had an impact on the types of surveys acquired in areas with a high geologic complexity. An example of this is the optimization of acquisition in the Gulf of México (GOM) with sparsely sampled Ocean Bottom Nodes (OBN) (eg., Huang et al. 2023). In some cases, the combination of a sparse OBN survey with legacy streamer data takes advantage of the long to super-long offsets from the OBN data for model building and the dense near-offset sampling of available legacy streamer data to produce high-quality images. Huang et al. (2020) demonstrated the use of acoustic FWI with a sparse OBN data from the GOM resulting in a higher quality model and image in the subsalt region compared with previous results obtained from the available streamer data. In that sparse OBN survey, the nominal node spacing was 1 km by 1 km and the source spacing was 50 m by 100 m in the inline and cross-line directions, respectively. The maximum nominal offset was 40 km, necessary for resolving the velocity model deeper than 10 km, and the final model was obtained for a maximum frequency of 12 Hz. This demonstrated the advantages of using such sparse node data with ultra-long offset, through a multi-stage approach.

In regions characterized by a strong impedance contrast, such as a shallow salt environment, the Earth's elastic properties pose challenges for acoustic FWI. Often, acoustic FWI yields velocity models with unfocused interfaces, due to inaccuracies in acoustic modeling at boundaries (Plessix et al., 2021). Even when only inverting the pressure wavefield recorded by the hydrophone component, performing elastic propagation benefits the inversion process due to a more accurate representation of the underlying physics. Elastic modeling in complex geologic areas can be computationally challenging due to factors such as strong contrast interfaces and boundaries, or very low shear wave velocities. Various approaches have been proposed to accurately model shear waves near the water bottom (van Vossen et al. 2002, Macesanu 2020, Singh et al. 2021). In the case of pressure wave modeling, we find that density variations can also have a significant effect. In the case of a strong contrast at an interface, the kinematics of the pressure wavefield modeled on a staggered grid can exhibit an anisotropic effect manifested as a change in velocity in a direction perpendicular to the interface. This effect is proportional to the finite difference (FD) grid size, thus being significant at low frequencies, which are important for FWI updates. Two strategies can mitigate this issue: adopting a staggered grid definition for the density model or employing a modified version of the stress-velocity equations. In the following sections, we discuss the implementation of elastic FWI and showcase results based on a sparse OBN survey conducted in the GOM.

Theory

The elastic wave equations in a stress-velocity formulation read

$$\frac{\partial \tau_{ij}}{\partial t} = c_{ijkl}\frac{\partial v_k}{\partial x_l} + I_{ij}(x) \qquad (1)$$

$$\frac{\partial v_i}{\partial t} = \frac{1}{\rho}\frac{\partial \tau_{ij}}{\partial x_j} \quad .$$

These equations are solved numerically by representing the dynamic (physical) fields (6 stress tensor components τ_{ij} and 3 vector component velocities) and the model fields (the stiffness tensor c_{ijkl} and density ρ) at discretized locations in space. The standard FD approach employed in the implementation of elastic equations (Virieux, 1986) uses

staggered grids, with the diagonal stresses τ_{ii} being sampled on the reference grid, while the velocity fields and off-diagonal stresses are sampled on grids shifted by half interval with respect to the reference one.

The accuracy for solving equation (1) with the FD method relies on the dynamic fields and the model properties being relatively smooth on a scale comparable to the grid sampling. However, the primary interest for solving the elastic equations relates to targeting subsurface geology characterized by a high degree of heterogeneity such as the water-sea floor contact and sedimentary-salt interfaces. Let us consider for example density variations, which are most significant near the seafloor. In an acoustic isotropic medium, for simplicity, the equation for the pressure ($p = -\tau_{ii}$) can be written as

$$\frac{\partial^2 p}{\partial t^2} = \lambda \left[\frac{\partial}{\partial x_i}\left(\frac{1}{\rho}\frac{\partial p}{\partial x_i}\right) \right] \qquad (2)$$

$$\frac{\partial^2 p}{\partial t^2} = \frac{\lambda}{\rho}\nabla^2 p + \lambda\left(\frac{\partial b}{\partial x_i}\right)\frac{\partial p}{\partial x_i} \quad , \qquad (3)$$

with λ being the bulk modulus and $b=1/\rho$ the buoyancy. In this latest form, the right-hand part contains a kinematic term (proportional to the square gradient of the field) and a source term, proportional to the derivative of the model density/buoyancy (model reflectivity). The kinematic term implies the local velocity of the P wave is $v^2 = \lambda/\rho$. In the continuous limit, Equations 2 and 3 are the same. Their discretized forms, however, may be different. For example, in the case of implementation on staggered grids, the discretized equation for pressure in Equation 2 becomes

$$\frac{\delta^2 p}{dt^2} = \lambda \left[\frac{\delta_-}{dx_i}\left(\frac{1}{\rho_+}\frac{\delta_+ p}{dx_i}\right) \right] \quad , \qquad (4)$$

where δ_+, and δ_- are the forward and backward first order finite difference operators, respectively. The density field (and therefore buoyancy) is evaluated on the staggered grid $x_+ = x_i + dx_i/2$, while the bulk modulus is evaluated on the standard grid (x_i). Thus, for the staggered grid implementation, it can be shown that the kinematic term for pressure has the form

$$\frac{\lambda}{\rho}\nabla^2 p \rightarrow \lambda_k \frac{1}{2}\left[\left(b_{k-\frac{dx}{2}} + b_{k+\frac{dx}{2}}\right)\frac{\delta^2 p}{dx^2} + \left(b_{k-\frac{dy}{2}} + b_{k+\frac{dy}{2}}\right)\frac{\delta^2 p}{dy^2} + \left(b_{k-\frac{dz}{2}} + b_{k+\frac{dz}{2}}\right)\frac{\delta^2 p}{dz^2}\right] \quad , \qquad (5)$$

where δ^2 is the second order finite difference operator. Thus, depending on how the buoyancy terms are defined on the staggered grids, the kinematic term may be locally anisotropic. The input for the discrete problem is a buoyancy field defined on the main grid (b_k), with the values at staggered grid locations being evaluated through interpolation: $b_{k+dx/2} = (b_k + b_{k+dx})/2$. Therefore, the numerical directional P wave velocity at point k will be dependent on the smoothed buoyancy field

$$V_i^2(x_k) = \frac{\lambda_k}{4}\left(b_{k-dx_i} + 2b_k + b_{k+dx_i}\right) \quad . \qquad (6)$$

Based on this analysis, it appears the propagation will be isotropic for a relatively smooth input buoyancy field, however in the vicinity of a strong interface the effective velocity in the direction perpendicular to the interface will be modified; increased on the side with lower buoyancy (smoothing increases local buoyance) and decreased on the opposite side.

One approach which would partially address this problem involves using the input buoyancy defined on the grid staggered in the direction corresponding to the largest discontinuity. Since the strongest interface for density is the water bottom, and this is often close to horizontal, using the grid staggered in the z direction would typically be a good choice. Then the other quantities on the main grid are defined in terms of the physical observables v_p, v_s, and the average of $b_{k+dz/2}$. If the model is smooth enough in the x and y directions, the discretized equations will be kinematically accurate for all propagation directions.

Another solution to this problem is to reformulate the elastic equation such that reflectivity is separated from kinematics, similar to Equation 3. For this purpose, we define an effective stiffness tensor

$$c^0_{ijkl} = c_{ijkl}\frac{\rho_0}{\rho} \quad , \qquad (7)$$

with ρ_0 being constant density in water. We obtain then the following form of the elastic equations

$$\frac{\partial \tau_{ij}}{\partial t} = c^0{}_{ijkl}\frac{\partial v_k}{\partial x_l} - c^0{}_{ijkl}\frac{1}{\rho}\frac{\partial \rho}{\partial x_l}v_k + I_{ij}(x) \qquad (8)$$

$$\frac{\partial v_i}{\partial t} = \frac{1}{\rho_0}\frac{\partial \tau_{ij}}{\partial x_j} \quad ,$$

where the contribution of the variable density ρ appears as a reflectivity source term in the updated stress. Taking the time derivative of the stress and replacing the velocity terms from the second equation shows that systems (1) and (8) remain the same for the stress components. The advantage of this formulation is that kinematics of the wavefield becomes independent of the density ρ. Moreover, an additional benefit is that input parameters to the equations are given in terms of quantities (reflectivities) which may be more easily estimated (or inverted) than density (Whitmore et al., 2020; McLeman et al., 2021).

Elastic FWI for OBN surveys

For an illustration of the problem described above, we use a constant velocity model with v_p being 1500 m/s, and generate snapshots using both constant and varying density (for the varying density model, we use a simple step-like function to represent the seafloor interface, with ρ = 1 g/cm^3 in water and ρ = 2 g/cm^3 below). To simulate reciprocal OBN acquisition, we place the source at the water bottom, set at a depth that aligns with a multiple of the grid sampling to simplify source insertion. The input signal is a Ricker wavelet with a peak frequency of 6 Hz, and the numerical computation is done employing a 40 m grid sampling. Figure 1a shows a sample snapshot computed with constant density to serve as a base case, and next to it wavelets extracted from the red rectangle in the snapshot (Figures 1b, 1c, 1d), with a red wavelet indicating the base case and a green one the variable density case. For Figure 1b, the standard implementation is used (density specified on the standard grid), and a speedup of the down-going wave (the green wavelet) can be observed (corresponding to a time shift of about 2 ms). The wavelets obtained using density specified on a staggered grid and elastic equations with reflectivity source terms are plotted in Figures 1c, 1d, and show improved kinematic agreement with the constant density case.

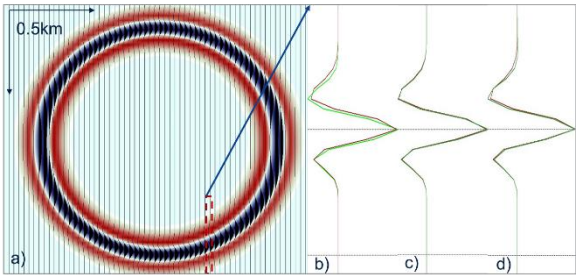

Figure 1 : a) snapshot computed with variable density (wiggles) overlaid on snapshot computed with constant density (color). Right panels: wavelet comparison for b) density defined on the main grid, c) density defined on the staggered grid and d) equations with reflectivity source terms.

Field data results

The real data example originates from a sparse node survey acquired in the Gulf of Mexico. This survey has a maximum nominal offset of 60 km, with a shot separation of 50 m by 50 m. Dynamic Matching FWI (DM FWI) (Mao et al., 2020) is applied to the hydrophone component after denoising such as deblending and simple swell noise removal. DM FWI uses a weighted local window cross-correlation based objective function that maximizes the similarity between the two datasets, the field data and a synthetically computed one, to estimate the misfit/residual and update the velocity model. The first frequency band inverted is below 2.5 Hz. The starting model is a smoothed version of a legacy velocity model derived from streamer data. The density and shear wave velocity models are derived from empirical relations based on well data in the GOM and following the bathymetry at the water bottom.

Both acoustic and elastic inversion were performed for a maximum frequency of 5 Hz, for assessing differences introduced by elastic propagation with respect to acoustic at relatively low frequencies. Figures 2a and 2b show the inverted velocity models from the sparse OBN data overlaid on the migrated stacks generated with the denser WAZ shots, for the acoustic and elastic inversions, respectively. The elastic FWI result shows improved resolution of the salt bodies from the better match of the elastic propagation implementation, compared to the acoustic case. A depth slice comparison of the migrated images also shows clear improvements in the sediment-salt boundary when using the elastic FWI model (Figure 2c) versus using the acoustic FWI model (Figure 2d). The improved data match for the elastic inversion is corroborated by the window averaged zero-lag correlation maps between synthetic and field data displayed in Figure 3 for the acoustic (a) and elastic (b) cases. Notably, the correlation coefficient is higher for the elastic case, signifying improved convergence and a better fit for the elastic result. The fact that these differences are observed at relatively low frequencies points towards convergence gains from using elastic propagators when building the long-wavelength component of the velocity field.

Conclusions

Elastic FWI offers strong benefits for model building in areas with high heterogeneity such as shallow salt geobody provinces. Elastic FWI requires considering the extra model parameters of shear wave velocity and density, as well as an accurate synthetic simulation engine. Finite differences modeling using density defined on the standard grid can lead to kinematic errors in areas with sharp contrast interfaces. Defining the density field on a staggered grid reduces errors in the propagation of the wavefield. As an alternative, we propose a modified form of the elastic equations, where the variable density contribution is expressed in terms of reflectivity, which also improves kinematic accuracy. Inversion results using a sparse OBN survey demonstrate the benefit from elastic FWI early in the model building process, as the long wavelength components of the velocity are sensitive to elastic effects, with a positive impact on the derived models and images.

Acknowledgements

The authors thank Bin Wang, Paul Farmer and Adriana Citlali Ramirez from TGS for discussions and supporting the

work. We also thank TGS Multiclient for the permission to publish the results.

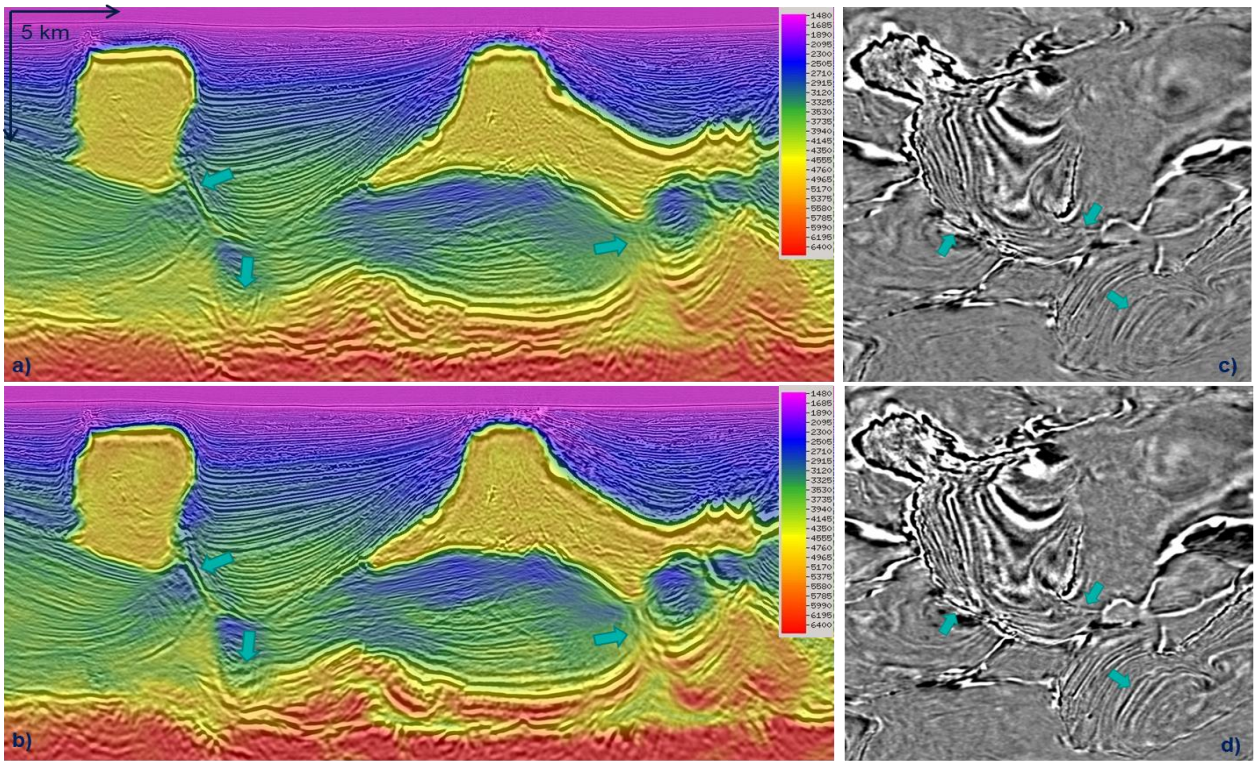

Figure 2: Migration stacks and velocity models obtained through acoustic (a) and elastic inversions (b). A depth slice of the image volume from acoustic inversion velocity model (c) and elastic inversion model (d).

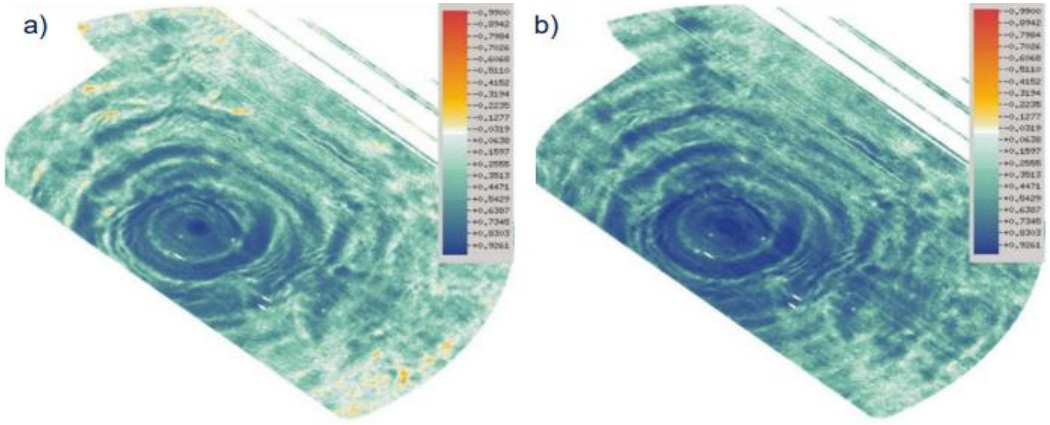

Figure 3: Cross-correlation map for one node gather, evaluated between field data and modeled synthetic from acoustic inversion (a) and elastic inversion (b).